

**2018 NDIA GROUND VEHICLE SYSTEMS ENGINEERING AND TECHNOLOGY
SYMPOSIUM
AUTONOMOUS GROUND SYSTEMS (AGS) TECHNICAL SESSION
AUGUST 7-9, 2018 - NOVI, MICHIGAN**

**IMPROVED RELATIVE POSITIONING FOR PATH FOLLOWING IN
AUTONOMOUS CONVOYS**

Thomas T. Tabb
Mechanical Engineering
Auburn University
Auburn, AL

Scott Martin, PhD
Mechanical Engineering
Auburn University
Auburn, AL

David Bevly, PhD
Mechanical Engineering
Auburn University
Auburn, AL

Jeff Ratowski
U.S. Army TARDEC
Warren, MI

ABSTRACT

This work presents the development of an algorithm to incorporate measurements from multiple antennas to improve the relative position solution between convoying vehicles provided by Global Positioning System (GPS) measurements. The technique presented, incorporates measurements from multiple antennas with a known fixed-baseline between a base antenna and auxiliary antenna on a base vehicle, and a rover antenna on a rover vehicle. The additional information provided by the fixed-baseline distance is used to provide an additional measurement with low uncertainty for improved integer ambiguity resolution between the base and auxiliary receiver, which in turn, provides additional measurements for determining the integer ambiguity difference between the base and rover receivers for the computation of a high-precision relative position vector (HPRPV).

INTRODUCTION

Autonomous vehicle convoying requires precise path following independent of the ability to maintain a constant line-of-sight between vehicles. Common technologies used for path generation, namely cameras and LiDAR, must be in view of the preceding vehicle and can be susceptible to debris like dust or smoke. Relative position determination provided by GPS techniques do not depend on maintaining a constant line-of-sight with

the leading vehicle and are negligibly affected by fog, dust, and smoke. GPS carrier phase observables are widely used to provide precise relative position solutions in kinematic applications. Changes in the carrier signal phase from epoch to epoch can be measured with an accuracy of 2-4 mm; however, the number of whole carrier cycles in the propagation path between the antenna and the satellite is ambiguous. Determining the number of whole carrier cycles in

the propagation path is known as carrier phase ambiguity resolution and is crucial for applications requiring centimeter-level positioning. In real-time applications, determination of the carrier phase integer ambiguities on-the-fly is required. A common technique applied to utilize the carrier phase measurement in real-time is differential GPS (DGPS). This approach removes error sources from the atmosphere, clocks, and ephemeris to more easily determine the bias in the measurement as a result of the integer ambiguities. Real-time kinematic positioning (RTK) is an application of DGPS that uses a static receiver, known as a base station, with a well surveyed global position, and a dynamic receiver, commonly known as a rover, that serve as the two receivers for differencing measurements. In this work, this concept is extended to the relative position between two vehicles without the need for a static base station, known as dynamic base real-time kinematic (DRTK) positioning. Improvements in the accuracy of the relative position solution and a reduction in the time required to fix ambiguities to a correct integer value (time-to-fix) by adding a measurement of a known fixed-baseline between antennas on a vehicle are explored. In this work, the coordinate system used is Cartesian earth-centered, earth-fixed (ECEF).

DRTK Overview

The DRTK method does not require a static base station to provide centimeter-level precision. This is advantageous for convoying where base stations are not available and where an available base station will lose efficacy after distances become too great for benefit (> 2 km) [3]. The traditional DRTK algorithm is a multi-step process that begins with the combination of pseudorange and carrier phase measurements from multiple receivers, as described in Equation (3-4), in a discrete, linear Kalman filter to estimate the relative ambiguities (float solution) between the receivers. Next, the floating-point estimates are fixed to integer values, and finally, the unambiguous carrier phase

measurements are used to compute a high-precision relative position vector (HPRPV) solution within a least-squares routine.

Measurement Models

Equation (1) is the measurement model of the pseudorange measurement. This measurement is effectively a measurement of the signal propagation time from satellite to receiver. This time interval is scaled by the vacuum speed of light to give distance in units of meters. The pseudorange observation between a user and satellite i can be related to the user position and clock states shown below.

$$\rho = |\mathbf{r}_i - \mathbf{r}_u| + c * b_u + \eta \quad (1)$$

\mathbf{r}_i is the satellite position at transmit time, \mathbf{r}_u is the receiver position at receive time, b_u is the bias in the receiver clock in seconds, c is the speed of light (m/s), and η is the combined error/noise attributed to atmospheric delays, satellite ephemeris mismodeling, and receiver noise [1]. Equation (2) is the carrier phase measurement model. Once the receiver locks on to a particular satellite, it keeps a running cycle count based on the Doppler frequency shift present on the carrier signal's respective frequency (L1, L2, etc.). The carrier measurement is more than one-thousand times less noisy than the pseudorange measurement [2]. The carrier phase observation between a user and satellite i can be related to the user position, clock states, and integer ambiguity N as shown below.

$$\varphi = |\mathbf{r}_i - \mathbf{r}_u| + c * b_u + \lambda N + \eta \quad (2)$$

The equation is in units of meters after scaling the measurement by the wavelength λ of the carrier signal, whether that be L1, L2, L5 etc. The benefit of the carrier phase measurement is the accuracy with which it can be measured; however, it is an ambiguous measurement and the bias from the integer ambiguities must be determined. A high-quality receiver is capable of measuring with an

accuracy of 1-2% of the wavelength [2]. The Coarse Acquisition (C/A) code from which the pseudorange measurement is determined, has a wavelength of roughly 300 meters and the carrier waves from which the carrier phase measurements are determined, have wavelengths of 19 centimeters and 24 centimeters for the L1 and L2 carrier frequencies, respectively [2]. After accounting for noise and resolution error, the 1σ values for the pseudorange measurement and carrier phase measurement are 1.5m and a couple of centimeters, respectively [2].

DRTK Algorithm

The DRTK algorithm exploits the accuracy of the carrier phase measurement to determine a relative position vector between two antennas. As in other DGPS techniques, the measurements between receivers are differenced to remove common atmospheric errors between the receivers, assuming the baseline distance is less than 2 km. A Kalman filter, described in **Figure 1** is used to iteratively estimate the ambiguities along with the geometry states and the clock bias. The pseudorange and carrier phase measurements from the rover and base are combined to perform the measurement update of the Kalman filter. The Kalman filter mean and covariance of the carrier ambiguities are then used to intelligently round the float estimate of the integer values using an algorithm called the Least-squares Ambiguity Decorrelation Adjustment (LAMBDA) method. Finally, the high precision RPV is calculated using the fixed integer value ambiguities and the carrier phase measurements from the two receivers [3]. The DRTK measurement models and state vector with Δ representing single-differenced measurements are below.

$$\Delta\rho = r_{r,b} + c * b_{r,b} + \eta_{r,b} \quad (3)$$

$$\Delta\varphi = r_{r,b} + c * b_{r,b} + \lambda N_{r,b} + \eta_{r,b} \quad (4)$$

$$X = [x_{r,b} \quad y_{r,b} \quad z_{r,b} \quad cb_{r,b} \quad N_{r,b}^1 \quad \cdot \quad \cdot \quad N_{r,b}^m]^T \quad (5)$$

The state vector includes the relative geometry states, $x_{r,b}$, $y_{r,b}$, $z_{r,b}$, the relative clock bias, $b_{r,b}$, and

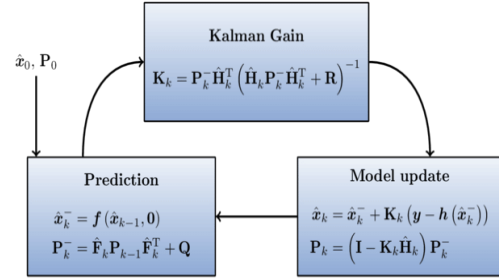


Figure 1: Kalman filtering routine.

the velocity states for $x_{r,b}$, $y_{r,b}$, and $z_{r,b}$ are also estimated but are excluded in Equation (5) for brevity. In Equation (3-5), the subscripts r, b denote that the parameter is the difference between the rover and base values, the superscript m is equal to the number of satellites observed, r is the true range to satellite. The noise values $\eta_{r,b}$ represent the noise characteristics of the single-differenced pseudorange and carrier measurements.

The observation matrix, Equation (6), consists of the unit vectors from satellite to receiver, and given that the baseline distance is sufficiently small, the unit vector a from the base to the satellites is sufficient to use in the model for both the base and rover. The dimensions of H are $n \times m$, where n is equal to the number of states estimated. Also, I is an identity matrix with dimension equal to $m \times m$.

$$H = \begin{bmatrix} a_x^i & a_y^i & a_z^i & -1 & 0_{mxm} \\ a_x^i & a_y^i & a_z^i & -1 & \lambda I_{mxm} \end{bmatrix} \quad (6)$$

The measurement vector is given in Equation (7) and consists of single-differenced pseudorange and carrier measurements between the rover and base receiver.

$$z = \begin{bmatrix} \Delta\rho_{rb} \\ \Delta\varphi_{rb} \end{bmatrix} \quad (7)$$

The state covariance matrix P is a diagonal matrix initialized with the expected variance of the initial estimates of the relative geometry and clock states

while the integer ambiguity states are set to an experimentally determined value of 0.5 [4]. The process noise covariance matrix Q is given below in Equation (8).

$$Q = \begin{bmatrix} Q_x & 0_{2 \times 2} & 0_{2 \times 2} & 0_{2 \times 2} & 0_{2 \times m} \\ 0_{2 \times 2} & Q_y & 0_{2 \times 2} & 0_{2 \times 2} & 0_{2 \times m} \\ 0_{2 \times 2} & 0_{2 \times 2} & Q_z & 0_{2 \times 2} & 0_{2 \times m} \\ 0_{2 \times 2} & 0_{2 \times 2} & 0_{2 \times 2} & 2Q_{cb} & 0_{2 \times m} \\ 0_{m \times 2} & 0_{m \times 2} & 0_{m \times 2} & 0_{m \times 2} & Q_N \end{bmatrix} \quad (8)$$

Q_x , Q_y , and Q_z are determined by the expected dynamics of the receivers and are treated as tunable parameters in this work. The integer ambiguity values, once the receiver maintains lock on the signal, are known to be constant with high certainty; however, to prevent the filter from disregarding new measurement information in the measurement update step, Q_N is given a fictitious process noise value of 1×10^{-6} . The clock term, Q_{cb} , is determined by the clock model for the receiver [5]. Additionally, the clock term is multiplied by 2 to account for the two respective clocks of the receivers.

The measurement noise covariance matrix R is given by the error model of the Delay Lock Loop (DLL) and Phase Lock Loop (PLL) of the receivers. The error models are given below.

$$\sigma_\rho^2 = \sigma_{\rho_{atm}}^2 + \sigma_{\rho_{DLL}}^2 \quad (9)$$

$$\sigma_{\rho_{DLL}} = \lambda_c \sqrt{\frac{4d^2 B_{np}(2(1-d) + \frac{4d}{Tc/n_0})}{c/n_0}} \quad (10)$$

$$\sigma_\varphi^2 = \sigma_{\varphi_{atm}}^2 + \sigma_{\varphi_{PLL}}^2 \quad (11)$$

$$\sigma_{\varphi_{PLL}} = \frac{\lambda_L}{2\pi} \sqrt{\frac{B_{n\varphi}(1 + \frac{1}{Tc/n_0})}{c/n_0}} \quad (12)$$

The parameters used in this work for the measurement error models are provided in **Table 1**. The carrier-to-noise-density ratio, c/n_0 , is

provided by the receiver and varies throughout the measurement period. The minimum ratio used in this work for acquisition is nearly 34 db-Hz and for tracking, 31 db-Hz [12].

Table 1: Pseudorange and Carrier Phase variance parameters [3].

Parameter	Description	Value
$\sigma_{\rho_{atm}}^2$	Atmospheric code delay	5.22 (m)
λ_c	Code chip width	293.05 (m)
d	Correlator spacing	0.5 (chips)
$B_{n\rho}$	Code loop noise bandwidth	2 (Hz)
T	Prediction integration time	2 (ms)
$\sigma_{\varphi_{atm}}^2$	Atmospheric carrier delay	0.03 (m)
λ_L	Carrier wavelength	L1, L2 (m)
$B_{n\varphi}$	Carrier loop noise bandwidth	18 (Hz)

Given this model, the measurement noise covariance matrix R is given in Equation (13).

$$R = \begin{bmatrix} \sigma_{r_{DLL}}^2 + \sigma_{b_{DLL}}^2 & 0 \\ 0 & \sigma_{r_{PLL}}^2 + \sigma_{b_{PLL}}^2 \end{bmatrix} \quad (13)$$

Equation (13) gives R for one satellite as a demonstration; in practice it will take on the dimension of two times the number of visible satellites on each frequency.

The next stage of RPV estimation is to fix the floating-point ambiguity estimates to integer values. The Kalman filter provides estimates of the single differenced integer ambiguities and a covariance matrix to describe the uncertainty in the estimates. Before implementing the LAMBDA method, the single differenced estimates are transformed into double differenced estimates to remove residual receiver clock errors that remain after single differencing. The double difference transformation is linear and performed by differencing all of the single-differenced estimates by one single-differenced estimate related to the satellite most directly overhead, because its signal is assumed to be the least affected by atmospheric delays [9]. In short, all estimates are differenced by one common satellite. Additionally, the covariance matrix P must be transformed. For example, this

transformation is performed on 5 satellites as described in Equations (14-16).

$$A_d^s = \begin{bmatrix} 1 & -1 & 0 & 0 & 0 \\ 0 & -1 & 1 & 0 & 0 \\ 0 & -1 & 0 & 1 & 0 \\ 0 & -1 & 0 & 0 & 1 \end{bmatrix} \quad (14)$$

$$\hat{N}_{dd} = A_d^s \hat{N}_{sd} \quad (15)$$

$$P_{N_{dd}} = A_d^s P_{N_{sd}} A_d^{sT} \quad (16)$$

After the integer values are fixed with the LAMBDA method, a HPRPV is calculated using least-squares as shown in Equation (17).

$$\vec{r}_{r,b} = (\Delta \vec{a}^T \Delta \vec{a})^{-1} \Delta \vec{a}^T (\Delta \nabla \varphi_{r,b} - \lambda \Delta \nabla N_{r,b}) \quad (17)$$

Where Δa represents the transformed unit vector from satellite to receiver to agree with the now double-differenced geometry, $\Delta \nabla \varphi$ represents the double-differenced carrier measurements between base and rover, and $\Delta \nabla N$ represents the double-differenced integer estimates [3].

Another common technique decouples the clock bias and position states from the model to exclusively estimate the integer ambiguity states. It will not be covered here, but can be found in [7,8].

Multi-Antenna DRTK Overview

Adding the measurement of the known, fixed-baseline between antennas on a single vehicle significantly reduces the time-to-fix and increases the accuracy of the HPRPV, because the initial float solution estimates are more accurate. This method provides the possibility of obtaining nearly the same performance as a dual-frequency receiver in the conventional hardware configuration and

algorithm with a low-cost alternative single-frequency receiver, simply because one may double the measurements without estimating additional states.

Convoy vehicles can be fitted with multiple antennas rigidly fixed to the frame of the vehicle. This work utilizes this configuration to provide a known baseline to resolve integer ambiguities between antennas on the same vehicle to provide more efficient carrier ambiguity resolution between convoy vehicles for computation of the HPRPV.

Fixed-Baseline DRTK Algorithm

The first step in using the known baseline information is to determine the relative integer ambiguity difference between the base and auxiliary receiver. After this solution converges and the integer ambiguities are fixed, one may use this information in a second Kalman filter to determine the distance between the base to the rover receiver. This implementation violates the white noise assumption of the Kalman filter because the estimation errors from the first filter are time-correlated. This is commonly known as the *cascaded Kalman filters* problem [5]. Treatments for this subject are covered in [5,10]. In this work, this violation is ignored in the second filter accepting the auxiliary measurements with colored noise, and the noise is treated as white; however, the auxiliary measurements are noisier as a result of adding a noisy measurement to another noisy measurement. This increase in noise is accounted for in the measurement noise covariance matrix.

The known baseline information is utilized by adding the low-uncertainty measurement of the baseline to the measurement vector. This constrains the low-precision baseline estimates to a circle with radius equal to the baseline magnitude (see **Figure 2**) [3]. The following row must be appended to the observation matrix.

$$H = \begin{bmatrix} \frac{x_{r,b}}{\rho_b} & \frac{y_{r,b}}{\rho_b} & \frac{z_{r,b}}{\rho_b} & 0 & 0_{1 \times m} \end{bmatrix} \quad (18)$$

The baseline ρ_b and observation matrix are calculated with the current best estimates of the states as shown in Equation (19).

$$\rho_b = \sqrt{x_{r,b}^2 + y_{r,b}^2 + z_{r,b}^2} \quad (19)$$

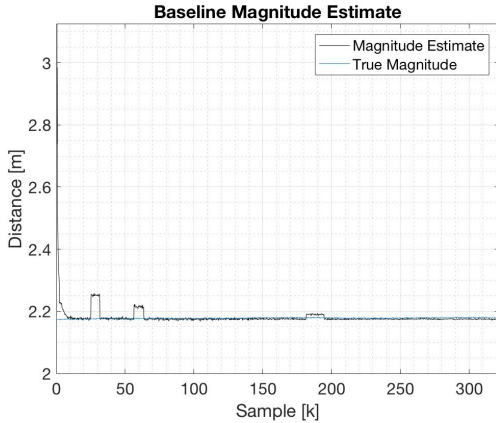


Figure 2: Constrained baseline estimates.

Additionally, the measurement covariance matrix R must be altered to include the certainty with which the fixed baseline was measured. If measured with RTK, this value is 0.01 cm^2 [3]. After the integer ambiguities between the auxiliary receiver and base receiver are resolved, this information can be passed to the second Kalman filter which takes advantage of the known geometry to provide additional measurements without the burden of estimating additional states [6].

Multi-Antenna DRTK Algorithm

The additional measurements provided by the known-baseline information are derived using simple vector addition as described in **Figure 3**. By vector addition, the new measurement vector z is derived below in Equation (20-23).

$$\varphi_{23} = \varphi_{13} - \varphi_{12} \quad (20)$$

$$\begin{aligned} \widetilde{\varphi}_{13} &= \varphi_{23} + r_{12} + \lambda N_{12} + c * b_{12} \\ &= r_{13} + \lambda N_{13} + c * b_{13} \end{aligned} \quad (21)$$

$$\widetilde{\rho}_{13} = \rho_{23} + r_{12} + c * b_{12} = r_{13} + c * b_{13} \quad (22)$$

$$z = \begin{bmatrix} \rho_{13} \\ \widetilde{\rho}_{13} \\ \varphi_{13}^{L1} \\ \widetilde{\varphi}_{13} \end{bmatrix} \quad (23)$$

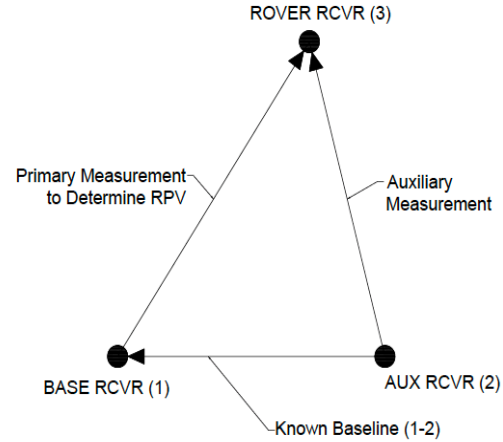


Figure 3: Description of receiver geometry

In this work, the estimates of the baseline integer ambiguity states are passed to the second filter in a cascaded architecture before integer fixing to begin estimation earlier.

Results

Pseudorange and carrier phase measurements were simulated in MATLAB with noise characteristics simulated as given in [1]. Monte-Carlo simulations were performed to validate the concept. The algorithms were all developed in MATLAB and the simulations were carried out with a sample frequency of 10 Hz. Additionally, the simulations were performed using L1 and L2 frequencies to simulate a dual-frequency receiver, and L1 alone to simulate a low-cost receiver. Statistics from the simulations were generated and comparisons were drawn based on time-to-fix to the correct integer, and error in the estimate. A display of the mechanics of the filter are shown in **Figure 4** as the estimates converge to the correct value on four satellites selected at random for this demonstrative figure. All integer ambiguities were

randomly generated. Next, raw GPS data was provided by TARDEC from a recent trial with convoying vehicles equipped with the appropriate fixed-baseline hardware configuration. This data was used to validate the algorithm’s performance and to confirm the veracity of the claims. The data provided was sampled at 5 Hz and contained dual frequency measurements. Global RTK solutions were used for comparison.

Static Simulated Data Simulation

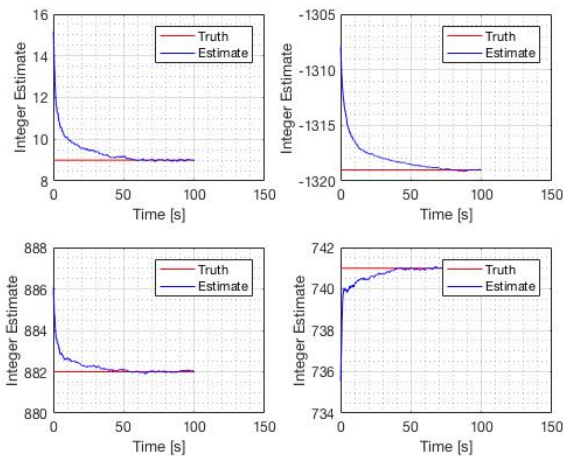


Figure 4: Integer ambiguity estimation mechanics.

Figure 4 shows the estimates converge to the correct value but converge slower than the statistics given in **Table 2**. This is because these values were taken directly from the Kalman filter float solutions before the LAMBDA method decorrelates the integer estimates and uses the error covariance to determine the correct integer.

Table 2: Performance statistics.

Multi-Antenna	Conventional
$\mu = 1.75 \text{ s}$	$\mu = 2.40 \text{ s}$
$\tilde{x} = 1.25 \text{ s}$	$\tilde{x} = 3.30 \text{ s}$
$\sigma = 1.40 \text{ s}$	$\sigma = 2.60 \text{ s}$

The multi-antenna approach provides a faster time-to-fix and is more closely distributed to the mean than the conventional algorithm with this simulated data.

Figure 5 and **Figure 6** compare the solutions in the RPV estimate provided by the LAMBDA method over the time of one simulation with the same randomly generated data. The LAMBDA method will provide integer estimates, regardless if they are correct, and a least-squares solution of the RPV can be calculated. It can be seen that the multi-antenna algorithm converges faster to the

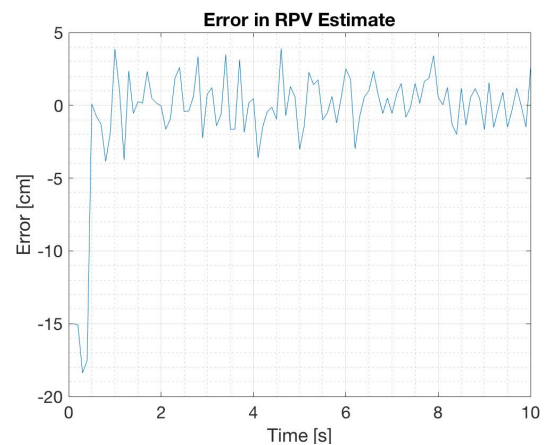


Figure 5: Multi-Antenna DRTK integer ambiguity estimation.

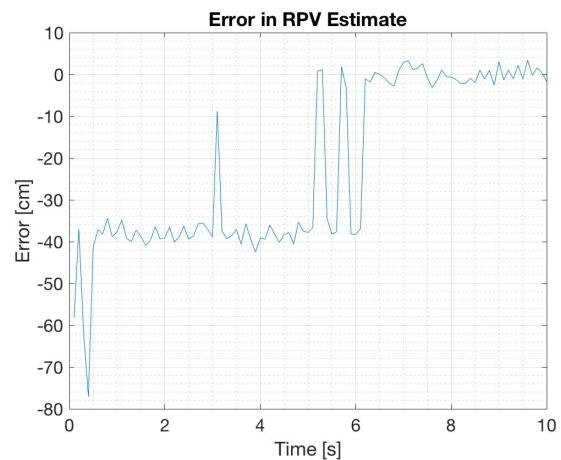


Figure 6: Conventional DRTK integer ambiguity estimation.

correct value, which in practice is determined by a statistical threshold known as the ratio test that

must be met. A common threshold is 3 [3]. In this simulation, the ratio test was not used for validation because the correct integers were known, so the performance of the filter could be directly observed. Additionally, the initial estimates of the RPV leading to convergence are better in the multi-antenna case. It is important to note that regardless of the method used, DRTK provides centimeter-level precision when fixed integers are available and even before, the estimates have sub-meter accuracy.

Dynamic Experimental Data Simulation

The results from the simulated data were confirmed when the algorithm exhibited the same behavior with experimental data. **Table 3** lists the results of the simulations with 10 minutes of dynamic data. These statistics include the total performance of the algorithm including periods when fixed integers were available (HPRPV) and when they weren't (float solution). The error was determined by comparing the solutions from the DRTK algorithms to RTK solutions provided by NovAtel's Waypoint® post-processing software.

Table 3: Total error in RPV estimation over 10 minutes including float solutions and fixed solutions.

Multi-Antenna Error	Conventional Error
$\mu = 1.83 \text{ cm}$	$\mu = 4.72 \text{ cm}$
$\sigma = 7.97 \text{ cm}$	$\sigma = 9.16 \text{ cm}$

The multi-antenna algorithm improved the time-to-fix by a factor of nearly 2. In this simulation the times-to-fix were 8.8 seconds and 15.6 seconds for the multi-antenna and conventional algorithms, respectively. It is important to note that the time-to-fix is heavily influenced by the value of the ratio used in the ratio test. A stricter ratio, higher in number, will increase the time-to-fix. In this simulation, the time-to-fix refers rather to the amount of time the filter takes to converge on the correct integer values that are validated by the error in the RPV estimate compared to the RTK truth

solution. The time-to-fix based solely on the ratio test was comparable for both the conventional and multi-antenna algorithm in this experiment.

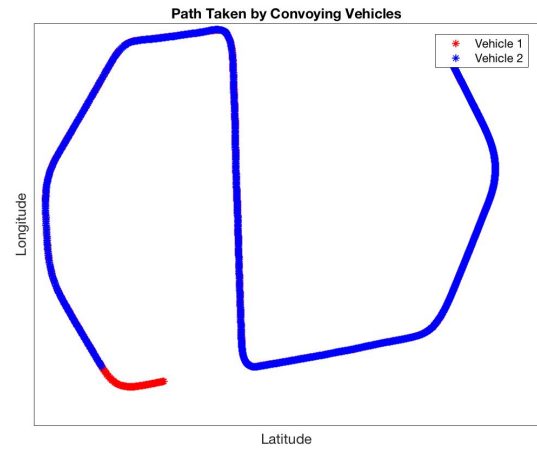


Figure 7: Path taken by vehicles in dynamic experimental data simulation.

Figure 8 depicts the convergence and error behavior of the multi-antenna and conventional algorithm. In this simulation, the LAMBDA method is used to continuously estimate the integers rather than fixing and holding the values after the ratio test is passed. For more on the ratio test, see [11].

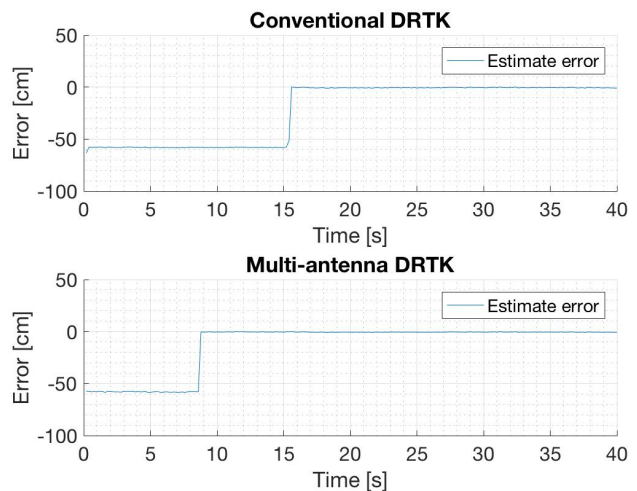


Figure 8: Total error comparison between the algorithms.

The float solutions are also improved upon with the multi-antenna algorithm. The error statistics are provided in **Table 4**.

Table 4: Float solution performance statistics.

Multi-Antenna Error	Conventional Error
$\mu = 37.01cm$	$\mu = 55.06 cm$
$\sigma = 8.72 cm$	$\sigma = 8.24 cm$

Conclusions

In this work, pseudorange and carrier phase GPS measurements were used to determine the relative positions of antennas, thus vehicles, in an autonomous convoy. The conventional DRTK algorithm was described and then compared to a new method incorporating measurements from a third receiver. The new method, multi-antenna DRTK, of incorporating measurements from an auxiliary receiver was developed and shown to perform more effectively based on the parameters of time-to-fix and overall error in solution. Additionally, the algorithm can be utilized in a low-cost implementation of three single-frequency receivers to provide comparable performance to the hardware configuration of two dual-frequency receivers.

Future Work

With the addition of a second antenna with known geometry fixed to a vehicle, attitude information may be calculated using GPS measurements. To improve the solution provided by stand-alone GPS, more measurements from radar, cameras, and an IMU can be fused in a Kalman filter to provide a more robust solution that is less susceptible to interference, multi-path effects, and signal loss. Additionally, this concept can be extended to an array of four antennas with known baselines of two pairs of antennas rigidly fixed to two separate convoying vehicles.

Acknowledgements

The authors wish to thank TARDEC for supporting this work and providing data for simulations.

REFERENCES

- [1] Parkinson, Bradford W., and James Spilker. "Global Positioning System: Theory and Applications", American Institute of Aeronautics and Astronautics, 1996.
- [2] Kaplan, Elliot D., "Understanding GPS: Principles and Applications", 1st ed., Artech House, INC. , 1996.
- [3] Martin, S. "GPS Carrier Phase Tracking in Difficult Environments Using Vector Tracking For Precise Positioning and Vehicle Attitude Estimation", (Dissertation). Auburn University, 2017.
- [4] Travis, W., "Path Duplication Using GPS Carrier Based Relative Position for Automated Ground Vehicle Convoys", (Dissertation). Auburn University, 2010.
- [5] Brown, R. G., & Hwang, P. Y., "Introduction to random signals and applied Kalman filtering: With MATLAB exercises", Hoboken, NJ: John Wiley & Sons, 2012.
- [6] Sperl, A., "Joint RTK and Attitude Determination", (Master's thesis). Technische Universität München, 2015.
- [7] Khanafseh, S. "GPS Navigation Algorithms for Autonomous Airborne Refueling of Unmanned Air Vehicles", (Dissertation). Illinois Institute of Technology, 2008.
- [8] Lawrence, D. "Aircraft Landing Using GPS: Development and Evaluation of a Real Time System for Kinematic Positioning Using the Global Positioning System", (Dissertation). Stanford University, 1996.
- [9] Misra, P., Enge, P. "Global Positioning System: Signals, Measurements, and Performance", Lincoln, MA: Ganga-Jamuna Press, 2011.

- [10] Bryson, A.E., and Johansen, D.E., “Linear Filtering for Time-Varying Systems Using Measurements Containing Colored Noise”, IEEE Transactions on Control, vol. 10, no. 1, pp. 4-10, Jan 1965.
- [11] Verhagen, S., and Teunissen, P., “The Ratio Test for Future GNSS Ambiguity Resolutions”, GPS Solutions, Online, 2012.
- [12] “OEMV® Family Firmware Reference”, NovAtel Incorporated, Calgary, Canada, 2010.